Korean J. Chem. Eng., 38(2), 411-421 (2021)
DOI: 10.1007/s11814-020-0726-8

pISSN: 0256-1115
eISSN: 1975-7220

Layer-by-layer of graphene oxide-chitosan assembly on PVA membrane surface for the pervaporation separation of water-isopropanol mixtures

Shivshankar Chaudhari*, KieYong Cho*, SoHyan Joo*, ByeongYun An*, SongEun Lee*, SeonYong Yun*, GiJung Lee*, JiHyeon Park*, MinYoung Shon*,†, and YouIn Park**

*Department of Industrial Chemistry, Pukyong National University, San 100, Yongdang-dong, Nam-gu, Busan 48547, Korea
**Center for Membranes, Korea Research Institute of Chemical Technology,
141 Gajeong-ro, Yuseong-gu, Daejeon 34114, Korea
(*Received 16 September 2020 • Revised 24 November 2020 • Accepted 30 November 2020*)

Abstract−A graphene oxide/chitosan polyelectrolyte layer was used to modify the surface of a polyvinyl alcohol/tetraethyl orthosilicate membrane by layer-by-layer interfacial complexation and, thus, improve the pervaporation characteristics. The interfacial complexation between the chitosan and graphene oxide was confirmed by Fourier-transform infrared and X-ray photoelectron spectroscopy; the changes in surface hydrophilicity after layer-by-layer modification were examined by contact angle measurements, and the morphology of the layer-by-layer membrane was elucidated by field-emission scanning electron microscopy analysis. The pervaporation performance of the modified membranes was evaluated by performing the separation of water-isopropanol (IPA) azeotropes under different operating conditions. In the pervaporation experiments, the best performance was obtained using a membrane with 15 chitosan-GO layers (denoted 15 L-L(CH-GO)). For this membrane, the flux increased from 13.6 to 76.4 g/m^{2}h and the separation factor decreased from 56,720 to 4,001 as the feed temperature was varied from 30 to 60 °C for an 80 : 20 (w/w) IPA/water feed. The apparent permeation activation energies were calculated and that of IPA (122.8 kJ/mol) was greater than that of water (47.4 kJ/mol).

Keywords: Poly(Vinyl Alcohol) (PVA), Chitosan, Layer by Layer, Graphene Oxide, Pervaporation, Surface Modification

INTRODUCTION

Isopropanol (IPA) is an industrial chemical that is used as a substitute for ethanol. IPA has an azeotrope with water at 87.7 wt% IPA content, yielding a mixture with a boiling point of 80.4 °C [1,2]. Therefore, IPA-water mixtures are often used as model feed systems to evaluate the pervaporation separation performance of membranes [3-5]. Convectional separation operation, such as a azeotropic distillation, is typically employed in the separation of IPA-water mixtures in the chemical industry. However, their energy-intensiveness makes them uneconomical. On the other hand, pervaporation separation is based on solution diffusion, and separation depends upon the difference in the adsorption and diffusion of components of a mixture, i.e., liquid mixtures are preferentially separated by phase changes through a membrane during mass transport [6-8]. As in the separation of azeotropes using distillation, pervaporation only requires the latent heat of evaporation of the permeates; thus, it is not limited by thermodynamics of vapor-liquid equilibrium. Therefore, pervaporation is a clean, economical, eco-friendly, and safe separation process [9,10].

Poly(vinyl alcohol) (PVA) is a promising membrane material, having excellent membrane forming character, physical robustness, and excellent chemical stability with organic solvents [11]. However, because of the abundant hydroxyl functionality in the PVA molecular backbone, PVA membranes swell easily in water [12]. Thus, methods like the chemical conjoining of PVA chains with cross-linking agent, grafting with polymer, mixing with polymers and thermal curing have been developed to prevent PVA membrane swelling [13-16]. The conjoining of PVA and tetraethyl orthosilicate (TEOS) to form an inorganic-organic composite can produce membranes with remarkable chemical and mechanical stability; crucially, these membranes can tolerate most organic alcohols and organic acid [17,18]. The condensation of PVA and TEOS occurs at mild temperature in the presence of an acid catalyst. Further, covalent bonding between the silicon containing compound (inorganic) and the PVA polymer (organic) is superficial. However, the introduction of a high content of a hydrophobic silicon based compound (in this case, TEOS) lowers the membrane water affinity, and this has a negative effect on the membrane performance. A promising technique to mitigate this hurdle is PVA membrane surface functionalization.

Hosseini and Nemati et al. coated a thin layer of super activated carbon nanoparticles (ACNs) -co-2 acryloamido-2 methyl propane sulfonic acid hydrogel layer on Polyvinyl chloride (PVC) based cation exchange based membrane. In their next study, they coated chitosan-co-activated carbon nanoparticles on the PVC-Co resin cation exchange membrane surface and used for heavy metal ions removal by electrodialysis. In both studies, they could have obtained excellent hydrophilicity at the membrane surfaces by modification with ACNs and hydrogel coating [19,20]. Meanwhile, surface mod-

†To whom correspondence should be addressed.
E-mail: myshon@pknu.ac.kr
Copyright by The Korean Institute of Chemical Engineers.

ification can also be achieved by the deposition of a layer of a polyelectrolyte complex (PEC) at the surface membrane. This layer deposition can result in a charged film surface, increasing the membrane hydrophilicity and polarity. Consequently, the surface of the modified membrane has a higher affinity for water than that of the unmodified organic membrane [21-23].

The solution diffusion model generally applies in polymeric membrane PV separation that explains molecule transport across the pervaporation membrane occurs via a series of steps: i) adsorption, ii) diffusion, and iii) desorption of permeates in the pervaporation [8]. In addition, it is well characterized that in determining the membrane selectivity toward a specific feed system adsorption plays crucial role [24,25].

There are two possible methods of modifying PVA base membranes: surface modification and bulk modification. There are several materials available for bulk modification, but surface modification remains underexplored. Nevertheless, surface modification by polyelectrolyte layers' deposition at the hybrid membrane (PVA/TEOS) surface is a potentially useful method, having benefits such as significantly enhanced water adsorption on the feed side of the membrane.

PECs are formed by electrostatic interaction between the polyelectrolyte polycations and polyanions [26]. In addition, two oppositely charged polyelectrolyte interaction is strong and instant, and the establishment of PECs is calibrated by both kinetic and thermodynamic factors. PECs are prepared by mixing polyelectrolytes, and the electrostatic forces between polyelectrolyte molecules result in the formation of PECs. In practice, this is represented by the contact between oppositely charged polyelectrolytes in a bulk phase [26,27]. Thus, PECs can be prepared in solution via the *mixing* or at an interface by *interfacial complexation* methods. One such interfacial complexation method is the layer-by-layer (LbL) method, which requires the use of polyelectrolyte solutions with low concentrations. In the LbL process, a substrate, such as a PVA-TEOS film, is exposed to polyelectrolyte solutions sequentially for a specified period, followed by thorough washing at intervals. Currently, a wide range of supports and assembly elements have been developed for the making of multilayer PEC membranes for pervaporation. As mentioned, the polyelectrolyte dipping solution concentration in the LbL method is very low, typically, 0.5 wt%, resulting in the slow growth of LbL films. As a result, a number of deposition layers are necessary to fabricate multilayered PEC membranes with considerable selectivity. Moreover, the morphology of multilayered PEC membranes is homogeneous. This is possibly due to the interfacial complexation in LbL films occurring at the molecular stages. Nevertheless, LbL membranes have been used to fabricate pervaporation dehydration membranes [28,29].

Chitosan, produced from of chitin by *N*-deacetylation, a natural and ubiquitous polysaccharide, is largely found in the exoskeleton of insects, fungi and crustaceans. Chitosan is a linear polymer consisting of glucosamine and *N*-acetyl glucosamine blocks via β-(1→4) linkages. The molar ratio of glucosamine to *N*-acetyl glucosamine, called deacetylation degree, is a significant character to determine its properties as well as applications. On deacetylation, chitosan can be dissolved in acidic media and only one polysaccharide that exhibits a high positive charge density; this is because of the protonation of the amine functionality on its backbone [29, 30]. In addition to this specific characteristic, it has been shown to have many other inherent properties, such as biocompatibility, non-toxicity, and biodegradability.

Graphene oxide (GO) is derivative of graphite produced by its oxidation via Hummer's method [31]. GO has a single honeycomb lattice thin sheet structure and contains many oxygen-containing functional moieties, such as polar hydroxyl and carboxylic acid groups, at the edges and epoxide groups on the basal plane. Additionally, GO with high mechanical strength can overcome the transport resistance through only one atom thick smooth surface. Therefore, the two-dimensional thin shape of GO enables GO to form layer by layer membrane. Moreover, the high content of polar oxygen functional groups results in a highly hydrophilic material as well as giving charge nature to GO. Therefore, it is possible to use GO to form a PEC via electrostatic interaction between oppositely charged polyions, i.e., (i) ionic crosslinking between ammonium in chitosan and carboxylate in GO [10], and (ii) hydrogen bonding between the protons in the carboxylic acids of GO and hydroxyl groups of chitosan [32]. The resulting polyelectrolyte complexes have increased charge density and high affinity toward water. Additionally, the formation of a stable chitosan coating layer at the PVA-TEOS surface is easy because the hydroxyl groups in both PVA and chitosan, as well as the amines in chitosan, can form strong hydrogen bonds with each other.

In this work, for the first time, we have developed PVA-TEOS membranes and modified their surfaces with a GO-chitosan PEC. The membrane performance was evaluated for the separation of water-IPA mixtures under various operating conditions. As per author's literature survey of concern, there is no such research which includes GO-chitosan layer by layer interfacial complexation on the PVA-TEOS membrane that has been examined till date.

EXPERIMENTAL SECTION

1. Materials

High-molecular-weight chitosan was procured from Sigma-Aldrich Co. (Iceland). Tetraethyl orthosilicate was procured from Sigma-Aldrich Co. (China). Poly(vinyl alcohol) with 98-99% hydrolysis degree (88,000-97,000, molecular weight) was purchased from Alfa Aesar (USA). Acetic acid (99.5 wt%) and IPA (99.5 wt%) were supplied by Dae-Jung Chemicals & Metal Co., Korea and were directly used after being received. Graphene oxide powder (15-20 sheets, 4-10% edges oxidized) was procured from Sigma-Aldrich Co. (USA). For the pervaporation experiments, different feed solutions were prepared from the appropriate mixture of IPA and water. For deionized water Puris Expe-RO EDI water system was used.

1-1. Preparation of PVA/TEOS Membranes

At higher concentration of PVA, the viscosity of the PVA solution was increased. Subsequently, it was difficult to cover the Petri dish surface completely as well as thicker membrane produced after drying; therefore, PVA concentration was limited to the 4 wt%. A 4 wt% of PVA solution was made by dissolving 4 g of PVA powder in 96 g of deionized water at 80 °C for 6 h. The obtained PVA solution was sonicated and degassed and kept at room temperature to remove the gas bubbles. Thereafter, 1 g of HCl was added

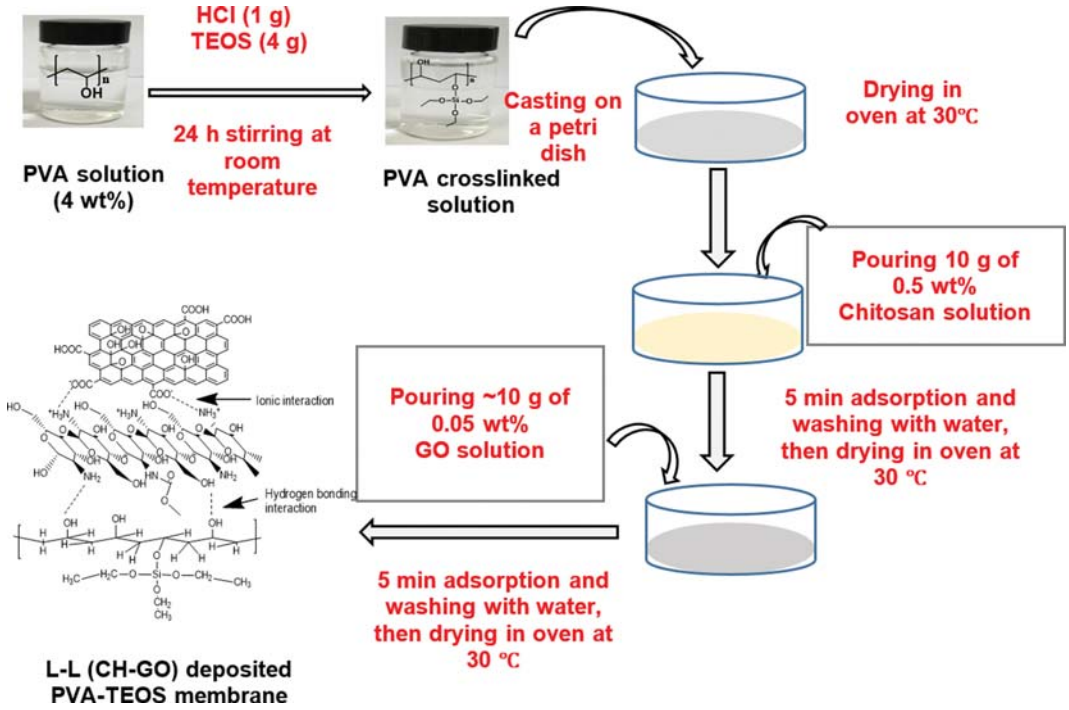

Fig. 1. Schematic diagram of layer by layer membrane preparation procedure.

to the PVA solution and was mixed about an hour. Subsequently, 4 g of TEOS was introduced to the reaction solution. The reaction solution was continually stirred for 24 h at ambient temperature. The condensation reaction occurs between the OH moieties in PVA and alkoxide groups in TEOS. Subsequently, the reaction mixture was filtered through an 80-mesh sieve to remove the unreacted material or particles formed during the reaction, and the solution was sonicated for 5 min and kept at room temperature to degas the mixture. Then, 10 g of solution was cast on a polystyrene petri dish and dried in an oven (Memmert, UN55) at 30 °C until completely dry. Finally, the membrane was immersed in fresh water to overcome an unreacted precursor. The obtained membrane is denoted 0 L-L (CH-GO), where CH indicates chitosan and GO indicates graphene oxide.

1-2. Preparation of the L-L (CH-GO) Membrane

The 0 L-L (CH-GO) membrane was flexible; thus, it was further modified by LbL coating with chitosan and GO. This was prepared by interfacial complexation. Briefly, 0.05 wt% was prepared by dispersing 50 mg of GO powder in 99.95 g of water followed by sonication at high intensity for 1 h. Similarly, a 0.5 wt% chitosan solution was made by dissolving 0.5 g chitosan powder in aqueous acetic acid (2 wt%) solution. To deposit the chitosan layer on the 0 L-L (CH-GO) membrane, 10 g of chitosan solution (0.5 wt%) was poured onto the top surface of the membrane and remained for 5 min to be adsorbed. Thereafter, the membrane surface was rinsed with copious amount of deionized water and allowed to dry in an oven (30 °C). After drying, 0.05 wt% GO disperse solution was deployed onto the membrane, likewise chitosan solution remained for 5 min and was rinsed with copious amount of deionized water (twice). The obtained membrane is named as a 1 L-L (CH-GO). A schematic diagram of L-L membrane preparation procedure is shown in Fig. 1. Membranes with different numbers of layers were prepared in the same way, and these L-L (CH-GO) membranes are denoted as per number of chitosan-GO layers: 5 L-L (CH-GO), 10 L-L (CH-GO), and 15 L-L (CH-GO). Brittle and cracked surfaces were formed when more than 15 chitosan-GO layers were deposited on the membrane surface, as depicted in Fig. 6(e). Thus, the L-L (CH-GO) deposition was limited to 15 chitosan-GO layers. The determined average thickness of the membranes was found to be 70-75 μm. A digital thickness gauge (Posi-Tector 6000) was used. For characterization, a PEC layer was also made using the same concentration of GO and chitosan solutions, as shown in inset of Fig. 6(e).

2. Characterization

The chitosan-GO PEC was subjected to attenuated total reflection (ATR)-Fourier-transform infrared (FTIR) spectroscopy (Nicolet iS10, USA). The spectra were recorded at wavenumbers between 400 and 4,000 cm^{-1}.

Thermogravimetric analysis (TGA) using a TGA 7 (Perkin Elmer, USA) of membranes was performed. The thermal degradation stability of the pristine PVA and PVA-TEOS membranes was examined. The membrane samples were conditioned to heating from 25 to 600 °C with heating rate (10 °C/min).

The cross-sectional morphology of all the membranes was studied by field-emission scanning electron microscopy (FE-SEM, Vega II, Tescan, Czech Republic). All the specimens were coated with platinum before analysis.

X-ray photoelectron spectroscopy (XPS) measurements of the 0 L-L (CH-GO) and 5 L-L (CH-GO), 10 L-L (CH-GO), and 15 L-L (CH-GO) membranes surfaces were carried out using Multilab 2000 (Shimadzu, Japan) and Kratos HP (Thermo VG Scientific, UK) spectrometers. A monochromatic X-ray (250-W Al K_{α}) source

was applied to achieve a 500-μm X-ray spot on the membrane sample. The analysis chamber pressure was maintained at 3×10^{-10} mbar. The XPS survey scans were carried out in 1.0-eV step with a pass energy of 160 eV.

The membrane surface hydrophilicity was determined by contact angle measurements. A Phoenix 300 contact angle analyzer (Kromtek, South Korea) assembled with a video camera was used. The sessile droplet method was used to calculate the contact angle of the water droplet on the membranes surfaces. For each measurement, 10 s after a drop of water was placed on the membrane surface, the contact angle was calculated. More than five measurements were performed at different positions over the membrane and the average values were reported.

3. Pervaporation Apparatus and Measurements

Pervaporation experiments for different feed mixtures were performed using an instrument designed in our previous study and shown in Fig. 2 [33]. The membrane for testing was cut to 7-cm diameter and placed in the membrane cell, which has two ends: an upstream side and downstream side. The upstream side is connected to the feed tank, whose temperature was maintained between 30 and 60 °C using an outer water circulation jacket. The feed solution was continually circulated through the cell (flow rate of 70 g/min) using a circulation pump (Model name) to avoid concentration polarization on either side of the membrane. The downstream side was connected to a permeate trap, where the permeate was frozen in a liquid nitrogen trap, and extended to the vacuum pump (Edwards, RV8). The vacuum pressure for all experiments was less than 10 mbar. As per the design of the membrane cell, the effective surface area of the membrane to be tested was 0.0019643 m^2, the run time for each experiment was 10 h, and the collected permeated solution was weighed using an electronic balance (Sartorius BA210S). A gas chromatograph (DS Sci. DS7200) consisting of flame ionization detector (FID) detector was used to determine the exact content of feed and permeated components. For accuracy, three successive pervaporation runs were carried out for each membrane sample, and the average value for each membrane was reported.

The membrane performance was evaluated by calculating the pervaporation flux (Eq. (1)), separation factor (Eq. (2)), and flux of individual components (Eq. (3)) for each membrane.

$$\text{Flux (J)} = \frac{Q}{A \times t} \tag{1}$$

where, J is the permeation flux (g/m^2h), Q is the mass of the permeate solution collected in the cold trap (g), A is the effective area (m^2), and t is the time (h).

$$\text{Separation factor } (\alpha) = \frac{P_{water}/P_{(IPA)}}{F_{water}/F_{(IPA)}} \tag{2}$$

where, P_{water}, $P_{(IPA)}$, F_{water}, and $F_{(IPA)}$ stands for weight fractions of water and IPA in the permeate and feed solution, respectively.

$$\text{Flux of an individual component } (J_i) = \frac{J \times P_i}{100} \tag{3}$$

where, J_i is for flux of component *i* (g/m^2h), and P_i is the weight fraction of component *i* (IPA, or water) in the permeate.

RESULTS AND DISCUSSION

1. Membrane Characterization

Fig. 3 shows the FTIR spectra of GO, chitosan, and the GO-chitosan complex. A broad band at 3,300-3,600 cm^{-1} correspond-

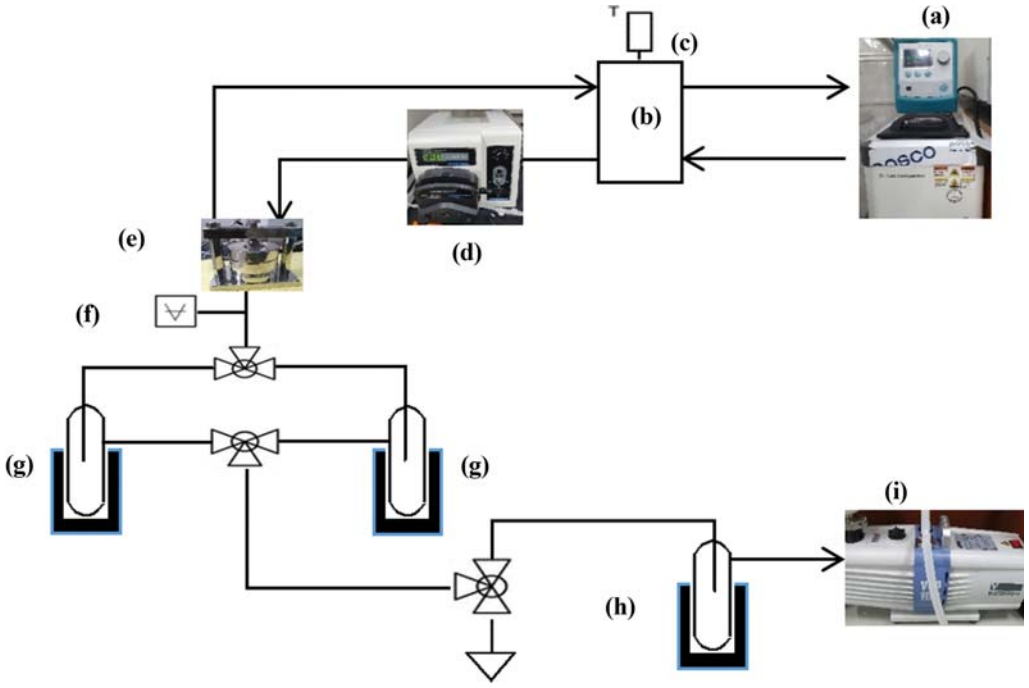

Fig. 2. Schematic diagram of pervaporation apparatus: (a) water bath (b) feed tank (c) temperature indicator (d) circulation pump (e) membrane cell, (f) vacuum gauge (g), (h) cold trap+liquid nitrogen (i) vacuum pump.

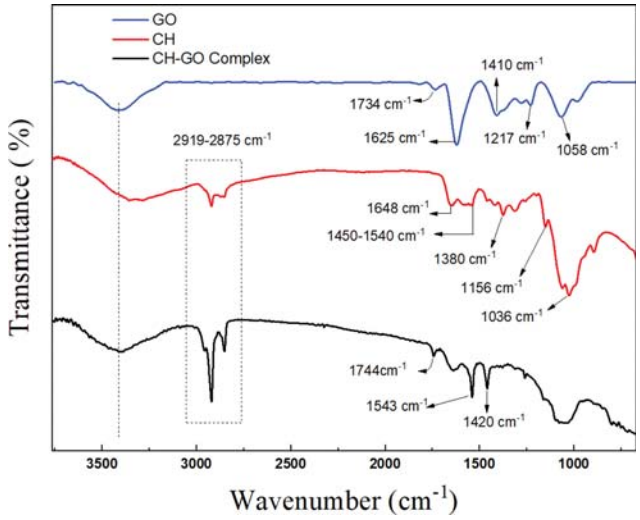

Fig. 3. FTIR spectra of GO, chitosan and Chitosan-GO complex.

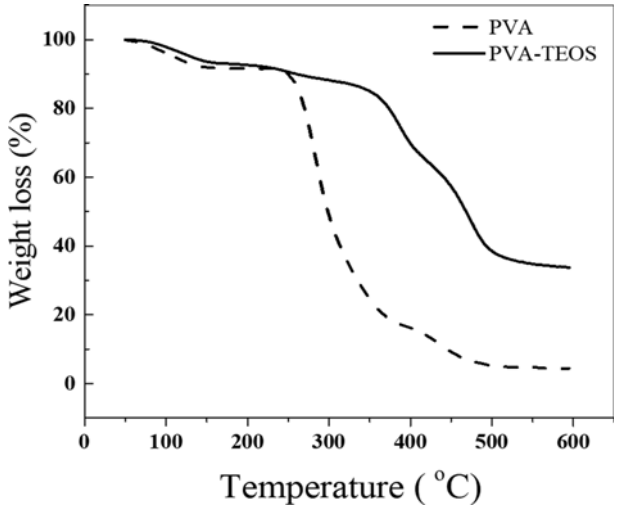

Fig. 4. TGA curves of pristine PVA and PVA-TEOS (0 L-L (CH-GO)) membranes.

ing to the O-H and N-H stretching vibration can be seen in the chitosan spectrum. The bands at 2,919 and 2,875 cm^{-1} correspond to the characteristic aliphatic C-H groups in chitosan. The stretching vibrational peaks at 1,648 and 1,380 cm^{-1} can be assigned to the C=O (amide I) and C-N (amide III) groups, respectively. Furthermore, the peaks at 1,540 and 1,450 cm^{-1} were assigned to the N-H bending vibrations of primary amines. Additional bands at 1,036 (O-H bending) and 1,156 cm^{-1} (C-O stretching) were observed [34]. Similarly, the spectrum of GO contains bands at 3,410, 1,058, 1,217, 1,410, 1,625, and 1,734 cm^{-1}, corresponding to OH stretching, C-O stretching, C-OH stretching, aromatic C=C stretching, C=O stretching, and COOH stretching, respectively [34-36]. In the spectrum of the GO-chitosan complex, the prominent peaks correspond to chitosan and GO, and some peak shift can be observed. The peak corresponding to C=O at 1,734 cm^{-1} in GO is slightly shifted to 1,744 cm^{-1}, whereas that at 3,474 cm^{-1} is shifted to 3,304 cm^{-1} because of the hydrogen bonding interactions of OH or NH_2 with C=O in GO [35]. Additionally, new bands corresponding to the asymmetric stretching of $-COO^-$ at 1,420 cm^{-1} and the bending of protonated amines (NH_3^+) at 1,543 cm^{-1} were observed. These results suggest the existence of electrostatic interactions between the carboxylate groups in GO and the ammonium groups in chitosan in the chitosan-GO complex [35,37].

The TGA curves of virgin PVA and PVA-TEOS membranes are shown in Fig. 4. For both the PVA and PVA-TEOS crosslinked (0 L-L (CH-GO) membranes, an initial weight loss of 5-10% occurred between 50 and 170 °C, assigned to the loss of physically bound water. Thereafter, two oxidative degradation steps were observed for both membranes. At 300 °C, the first weight loss of ~70% occurred caused by the loss of the PVA side chains. A second weight loss (~20%) occurred at 440 °C, resulting from the degradation of the main chain in the PVA membrane [38]. The TGA curve of the 0 L-L (CH-GO) membrane shows a shift in the temperature of the first weight loss to ~350 °C. Thus, the thermal stability of the 0 L-L (CH-GO) membrane was improved by the crosslinking between PVA and TEOS. This improved stability

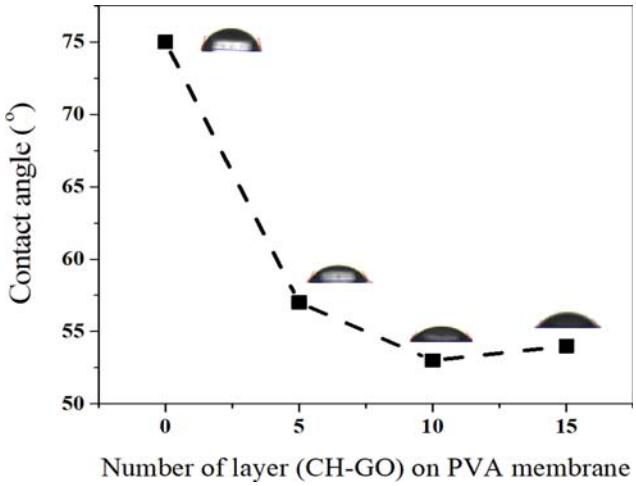

Fig. 5. Plot of effect of layer by layer CH-GO modification on contact angle of water at the membranes surfaces.

could be because the -Si-O- units in TEOS form covalent bonds with the hydroxyl groups in the PVA chain by condensation reaction. Thus, this result suggests the presence of a PVA-TEOS crosslinked network in the membrane.

To determine any changes to the surface hydrophilicity after the modification of the 0 L-L (CH-GO) membrane, water contact angles were measured. In Fig. 5, the water contact angles as a function of membrane composition are plotted. Compared to that of the 0 L-L (CH-GO) membrane, the water contact angle of the membrane modified with five chitosan-GO layers is reduced by 18° (from 75° to 57°). However, additional layers (10 L-L and 15 L-L) did not result in further reduction in the water contact angle. Thus, the hydrophilic moieties (NH_2, OH, and COOH) in chitosan and GO, as well as electrostatic interactions between COO^- and NH_3^+ increased the affinity of the membrane surface for water and improved the surface hydrophilicity of the membranes. These findings indicate that the modified membrane surfaces should have

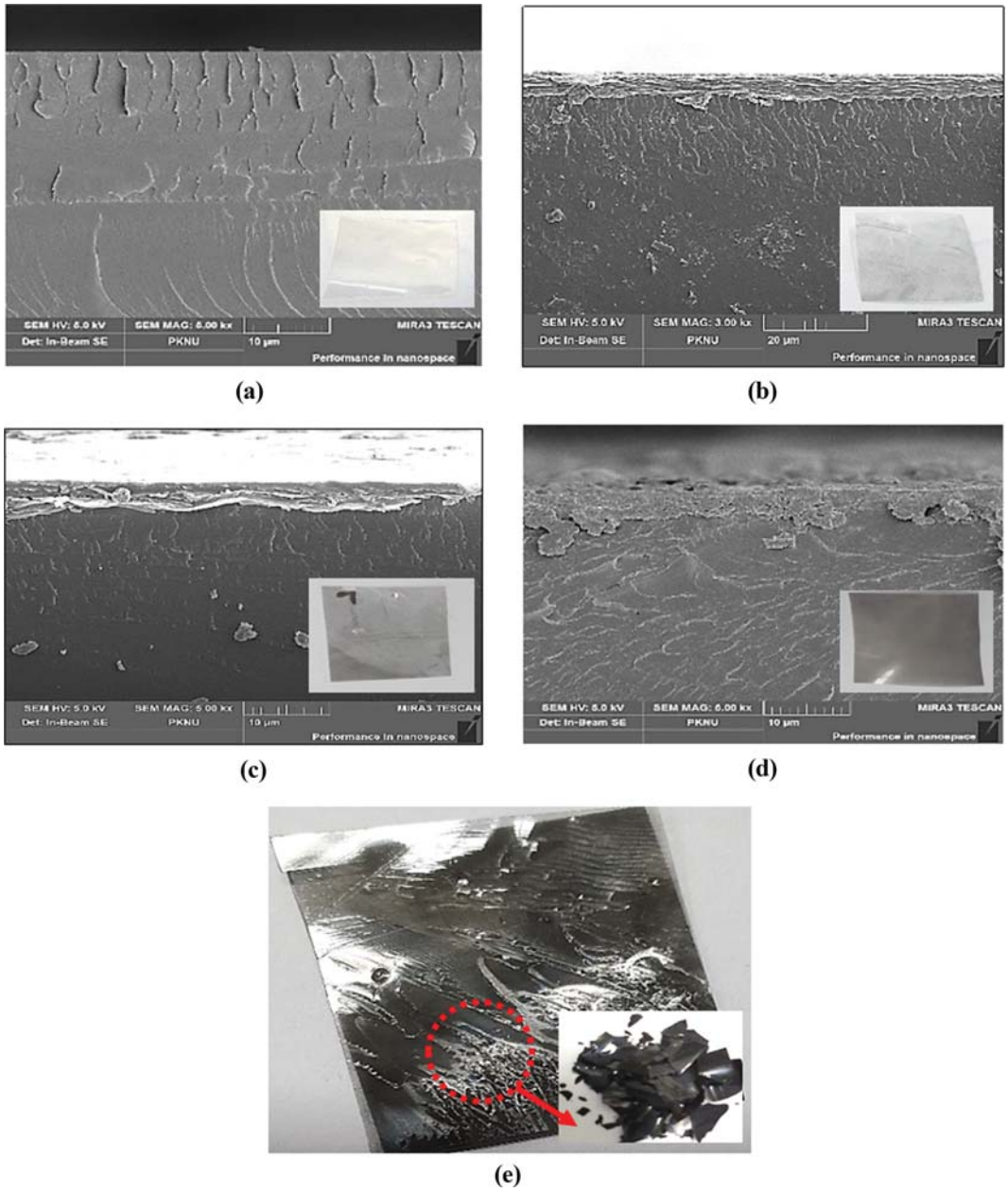

Fig. 6. Cross-sectional FE-SEM micrographs and real photos (inset) of PVA-TEOS membranes; (a) without CH-GO layer, (b) 5 L-L CH-GO, (c) 10 L-L CH-GO, (d) 15 L-L CH-GO and (e) 20 L-L CH-GO.

enhanced ability to adsorb water.

Fig. 6 shows cross-sectional FE-SEM micrographs of the membranes. A layer of chitosan and GO can be clearly observed on the homogeneous, dense PVA-TEOS membrane. From the micrographs, the thickness of the top layer in the 5 L-L (CH-GO) sample is 5-7 μm. Additionally, it can be seen that contact between PVA-TEOS and CH-GO layers are physical in nature and well connected to each other. At higher layers of CH-GO deposition, it can be observed that, the stratified structure of layers slightly changed to the dense structure, which can responsible for reduction in permeate rate.

Fig. 7(a) shows the XPS survey spectra of the pristine 0 L-L (CH-GO) and (5 L-L) (CH-GO) membranes. The spectrum of the 0 L-L (CH-GO) membrane contains two characteristic signals at binding energies (BEs) of 285 and 532 eV, corresponding to C 1s and O 1s in the PVA backbone, respectively [39]. On other hand, an extra peak at a BE of 400.9 eV assigned to N 1s was observed in the (5 L-L) (CH-GO) spectrum [40]. To confirm the interaction between COO^- in GO and NH_3^+ in chitosan, high-resolution XPS spectra of the N1s and O1s regions for the (5 L-L) (CH-GO) membrane were collected, as shown in Figs. 7(b) and 7(c), respectively. The N1s peak was deconvoluted into three regions. The peaks centered at BEs of 399.4, 401.7, and 405.6 eV correspond to the amine, protonated amine, and chemisorbed nitrogen in graphene oxide, respectively [41,42]. The O1s peak can be deconvoluted into four different signals. The peaks at BEs of 531.6, 532.6, 536.3,

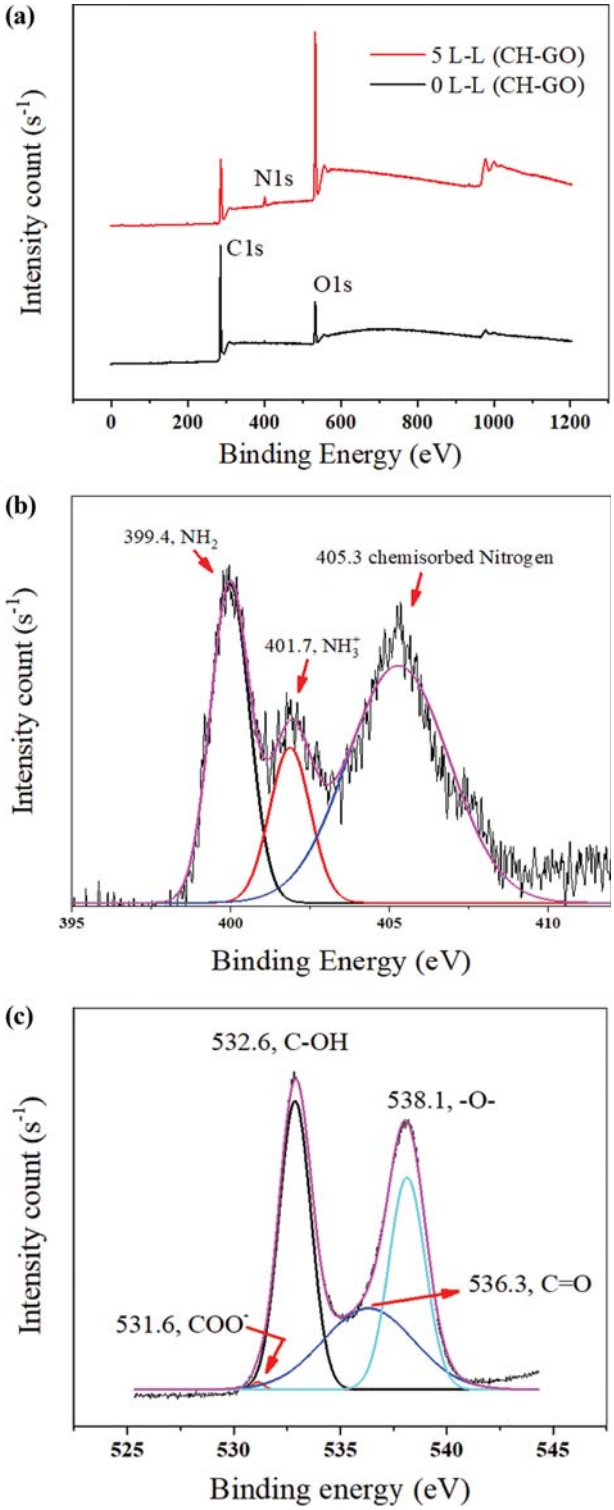

Fig. 7. (a) XPS spectra of 0 L-L (CH-GO) and 5 L-L (CH-GO) membranes and (b) XPS N1s core level spectra of 5 L-L (CH-GO) membrane (c) XPS O1s core level spectra of 5 L-L (CH-GO) membrane.

and 538.1 eV can be assigned to COO^- (carboxylate), -C-OH in either chitosan or GO [43], C=O [44] in GO, and ether linkages in the chitosan polymer, respectively. Therefore, based on XPS analysis, the presence of electrostatic interaction between GO and chitosan was confirmed, and a stable layer of the chitosan-GO PEC had been deposited on the membrane surface. On the basis of the FTIR, TGA, XPS, contact angle, and FE-SEM analyses, a schematic representation of the chitosan-GO membrane is proposed in Fig. 8.

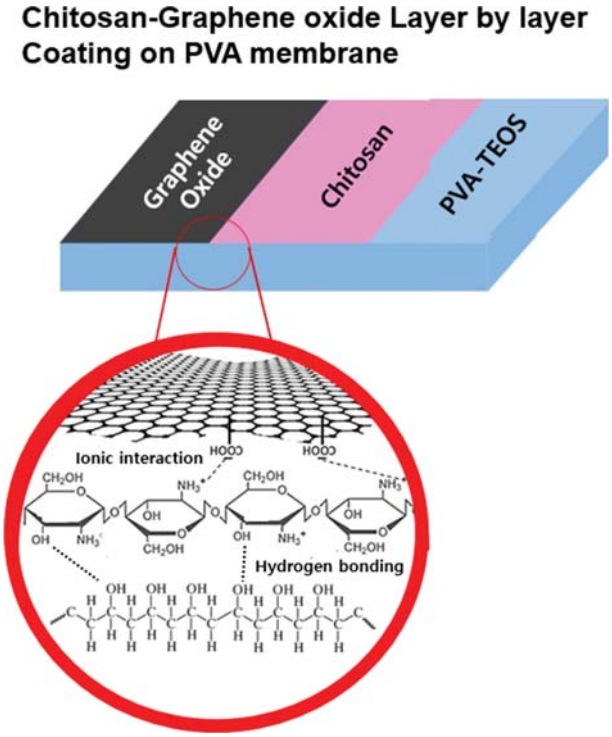

Fig. 8. Schematic representation of Chitosan-graphene oxide layer-layer membrane structure.

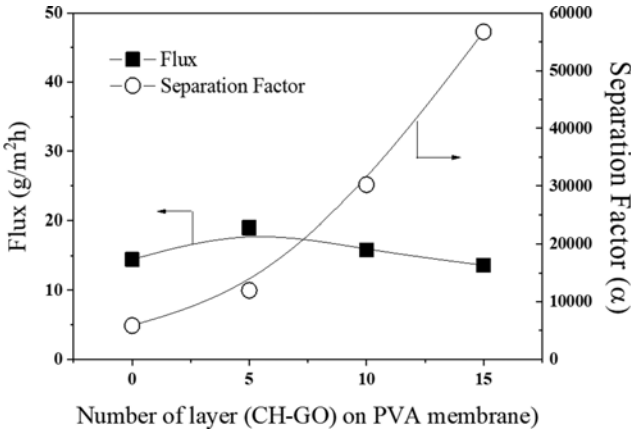

Fig. 9. Plot of pervaporation flux and separation factor a function of Chitosan-GO layer by layer compositions, feed composition 80/20 (w/w, %) IPA/water feed mixture at 30 °C.

2. Pervaporation Performance

To determine the effect of layer-by-layer chitosan-GO deposition on the pervaporation performance of the PVA-TEOS membrane, all membranes were tested for their pervaporation separation performance in IPA-water (80 : 20, w/w) feed mixtures at 30 °C. Fig. 9 shows the plot of the pervaporation flux (g/m^2h) and sepa-

ration factor (α) as a function of the number of chitosan-GO layers. There was no significant change in flux with layer number, and the fluxes of the 0 L-L (CH-GO), 5 L-L (CH-GO), 10 L-L (CH-GO), and 15 L-L (CH-GO) membranes were 14.45, 19.0, 15.8, and 13.6 g/m^{2}h, respectively. In contrast, the separation factors of the 0 L-L (CH-GO), 5 L-L (CH-GO), 10 L-L (CH-GO), and 15 L-L (CH-GO) membranes were 5,856, 11,962, 30,187, and 56,720, respectively, increasing with increasing number of layers from 5 to 15. Based on the solution diffusion model [8], pervaporation separation takes place via the adsorption of components at the membrane surface, followed by diffusion through a dense membrane and desorption under vacuum on the downstream side. Desorption is fast and the phase transition occurs across the membrane [45]. Therefore, the separation performance of the membrane depends on the affinity of the feed component for the membrane, as well as the size of the molecules.

In this study, after layer deposition, the water contact angle decreased, indicating that the hydrophilicity of the membrane surface had increased. This is likely because of the interaction between the OH and NH_2 groups, as well as the electrostatic interaction between COO^- and NH_3^+, in the polyelectrolyte layer. In addition, the higher polarity and charge density of the polyelectrolyte layer at the membrane surface favors the penetration of water over IPA [5,33,46]. Additionally, the stratified structure formed by the LbL deposition of GO and chitosan results in a tortuous path for permeating molecules [47]; this is especially true concerning the transport of IPA, which is large (kinetic diameter=0.47 nm). In contrast, water has a smaller kinetic diameter (0.296 nm) [48] and is highly polar, resulting in easy transport through the membrane. Thus, excellent water selectivity output was obtained after the LbL surface modification of the membranes.

Pervaporation is based on the difference in the chemical potential of the components on the feed and permeate sides of the membrane. Therefore, the membrane performance (flux and selectivity) is affected by changes in operating conditions, such as changes in feed composition or temperature [8]. Generally, an increase in the preferential component in the feed solution results in high membrane swelling (specifically for polymeric membrane) because of the plasticization of the polymer. This swelling increases the polymer void volume and, consequently, the flux increases and the separation decreases [49,50]. As the temperature increases, the vapor pressure on the feed side increases, while that on the permeate side remains the same. This results in the increased thermal motion of the polymer chain in the matrix and permeating components. Consequently, the free volume in the membrane increases, mass transport increases, and membrane selectivity decreases [2,27]. Figs. 10 and 11 show the effect of temperature and feed solution concentration on the flux and separation factor through the 0 L-L (CH-GO) and 15 L-L (CH-GO) membranes. The feed temperature was increased from 30 to 60 °C at 80 : 20 IPA-water feed content. The flux was found to be increased from 14.45 to 47.5 and 13.6 to 76.4 g/m^{2}h for 0 L-L (CH-GO) and 15 L-L (CH-GO) membranes, respectively. In contrast, the separation factor was reduced from 18,903 to 1,485 and 56,720 to 4,001 for 0 L-L (CH-GO) and 15 L-L (CH-GO) membranes, respectively. Similarly, when the water content in the feed was increased from 15 to 25 wt% at 60 °C (IPA and water

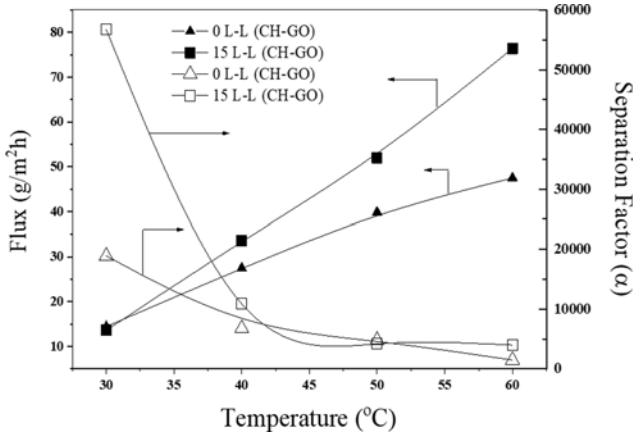

Fig. 10. Effect of temperature on flux and separation factor at feed composition 80/20, (w/w, %) IPA/water feed mixture.

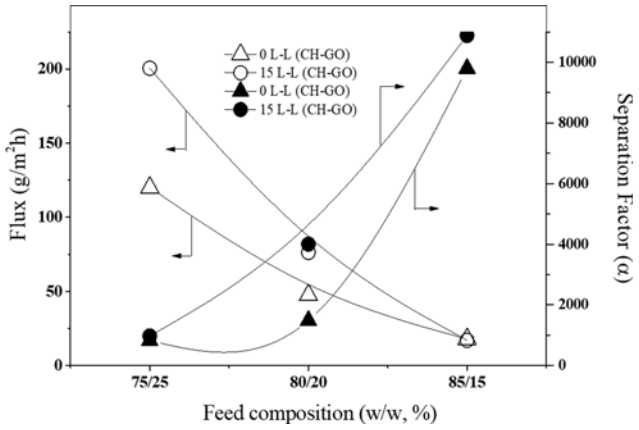

Fig. 11. Effect of feed composition on flux and separation factor at 60 °C.

form an azeotropic mixture within this range), the separation factor fell from 9,801 to 825 and 10,883 to 972, and the flux increased from 17.9 to 120 and 17 to 200 g/m^{2}h for the 0 L-L (CH-GO) and 15 L-L (CH-GO) membranes, respectively. Therefore, both membranes show typical pervaporation separation behavior on varying the operating parameters. Nevertheless, on the basis of the membrane performance, the surface modified membrane showed superior performance compared to that of the unmodified membranes, even on increasing feed temperature and water content in the feed.

The temperature dependence of the flux (J_i) can be expressed by Arrhenius-type Eq. (4) [51].

$$J_i = A_p \times e^{-E_a/RT} \quad (4)$$

where, A_p is a pre-exponential factor, E_a is the apparent permeation activation energy (kJ/mol), R is the molar gas constant (kJ/mol K), and T is the absolute temperature (K).

Fig. 12 shows a plot of the natural log of the individual fluxes of water and IPA as a function of temperature for the 0 L-L (CH-GO) and 15 L-L (CH-GO) membranes. Linear relationships between the fluxes and temperature were obtained for both membranes. From the slope of these plots, the permeation E_a was calculated;

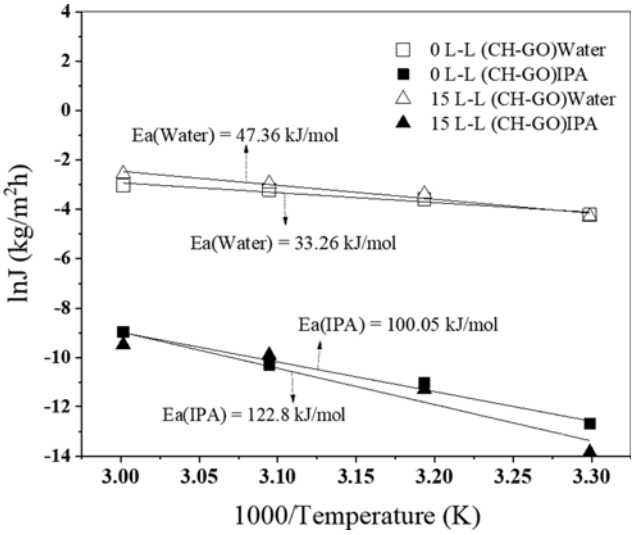

Fig. 12. Variation of $\ln J_{water}$ and $\ln J_{IPA}$ Flux as a function of temperature (K) at feed composition 80/20, (w/w, %) IPA/water feed mixture.

for IPA, E_a=100.05 and 122.8 kJ/mol and, for water, E_a=33.26 and 47.36 kJ/mol for the 0 L-L (CH-GO) and 15 L-L (CH-GO) membranes, respectively. The large difference in the permeation E_a values for water and IPA suggests the water-selective nature of the membranes.

The interaction between chitosan and GO layers is an ionic (physical) in nature; therefore, it is necessary to investigate the stability of L-L (CH-GO) membrane. Fig. 13 shows a stability study of 15 L-L (CH-GO) membrane. Since 15 L-L (CH-GO) has higher layers on its surface, it was chosen to observe a clear change in membrane appearance by the time of study. In the stability study, 15 L-L (CH-GO) membrane was weighed and immersed in the IPA/water (80/20, w/w) solution. Then it was sonicated for 10 minutes and put in the heating oven at 60 °C for five days. After every 24 h, the bottle was removed from the oven and sonicated for 10 minutes. Finally, membrane was dried in the vacuum oven and weighed. There was no significance change observed in the weight of membrane. Additionally, chitosan and GO complex on the surface of PVA was maintained with neither exfoliation nor extraction in feed solution, as can be seen from Fig. 13. Polyelectrolyte complex formed due to interfacial complexation between the chitosan (NH_3^+) and GO (COO^-); even though, it increases the hydrophilicity of the membrane but facilitates the physical cross-linking within layers that prevent the swelling in layers. Therefore, it is confirmed that, chitosan-GO complex is stable in IPA/water feed system for the given period of time. Meanwhile, in pervapo-

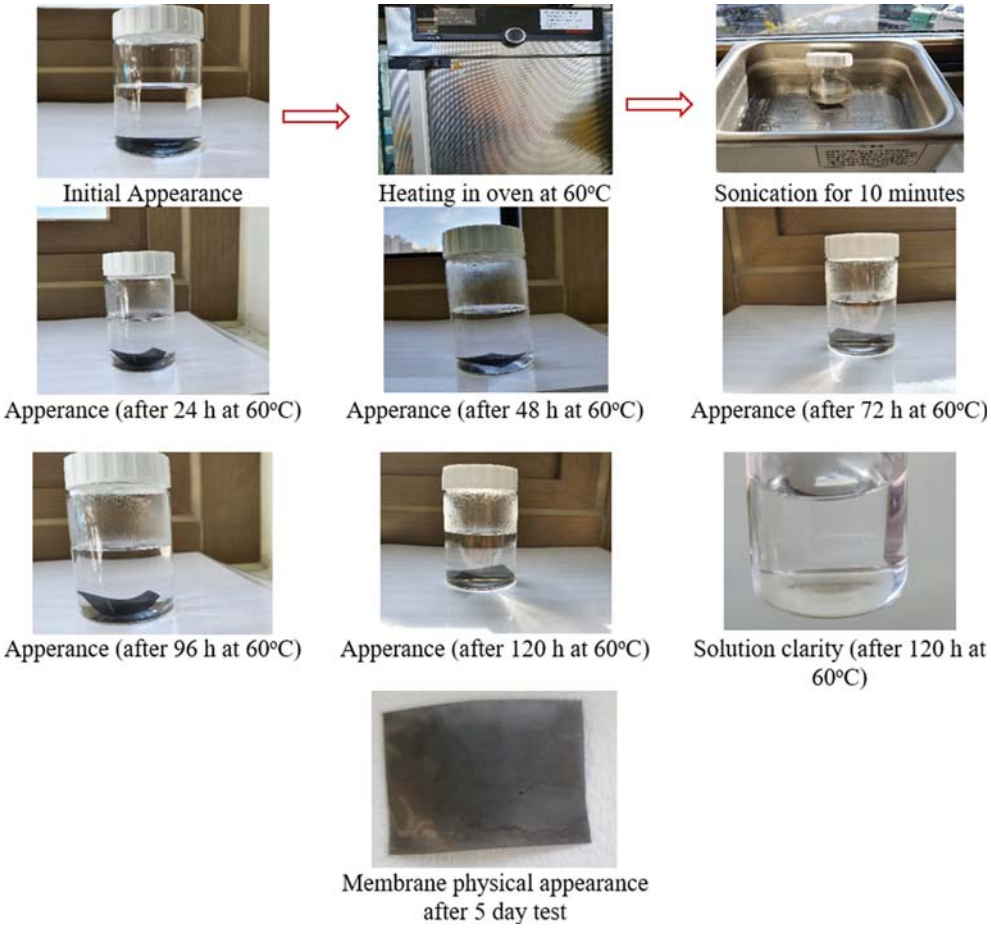

Fig. 13. Stability study of 15 L-L (CH-GO) membrane.

Table 1. Comparison table for pervaporation performance of 15 L-L (CH-GO) membrane with literature data for isopropanol pervaporation dehydration

Polymer	Nature of the membrane preparation method	Feed (%) composition, (w/w) isopropyl alcohol/water	Temperature (°C)	Flux (J) (g/m^2h)	Separation factor (α)	Thickness (μ)	Reference
PVA	PVA-GLU-Aluminosilicate (6 wt% filler)	12.5/87.5	40	110	73	50	[1]
PVA	PVA-blended-NaY zeolite	87.7/12.3	35	5.12	2,690	82	[2]
PVA	PVA-PNIPAAm Grafting	12/88	40	11	95	90	[13]
Chitosan	Chitosan-PSSAMA PEC membrane	87.7/12.3	60	54	1,313	40	[27]
Chitosan	Surface modification of chitosan with PBI	90/10	70	250	127	40	[52]
Matrimid 5218	Zeolite-5 (Si/Al=40, 10 wt% filled)	90/10	50	25	2,100	40-70	[53]
PVA	Surface modification (15 L-L (CH-GO)	80/20	60	76.4	4,001	70	This study
PVA	Surface modification (Chitosan-GO	85/15	60	17	10,883	70	This study

ration separation phenomenon, at downstream side (permeate side) of membrane the pressure is negligibly small (vacuum) and that additionally can help to prevent the layer's exfoliation from the upstream side of the membrane.

Table 1 shows the comparison of pervaporation performance of 15 L-L (CH-GO) membrane with that from literature data for isopropanol and water separation. It is observed that, the L-L approach remarkably improved the separation efficiency of membrane, but flux improvement was comparatively moderate to the research out in the literature. However, in pervaporation process, flux can be controlled with several factors, such as change in membrane module design to surface area enlargement, changes in processing parameter, reducing the active layer thickness by fabricating composite membrane with commercial porous support, e.g., polysulfone, alumina or polyvinylidene fluoride. Therefore, the properties at the PVA-TEOS membrane surface obtained from instant and strong interfacial complexation between Chitosan and GO provide a tunable surface functionality, suggesting that, by applying the above approach, these types of modification techniques have tremendous potential for fabricating future membranes.

CONCLUSION

Membranes with thickness ranging from 70 to 75 μm were prepared by the covalent crosslinking of PVA-TEOS, and the membrane surface was modified with chitosan and graphene oxide via layer-by-layer coating using the interfacial complexation method. All membranes were tested for their pervaporation separation performance with azeotropic mixtures of water and IPA. The best performance was obtained with the 15 L-L (CH-GO) membrane, which achieved a high separation (4001) and permeation rate (76.4 g/m^2h) in comparison to that of the unmodified 0 L-L (CH-GO) membrane (1,485 and 47.5 g/m^2h) at 60 °C for an 80 : 20 IPA-water feed. In conclusion, the layer-by-layer interfacial complexation of a chitosan-GO layer on PVA-TEOS membranes improves membrane hydrophilicity and allows the efficient dehydration of azeotropic mixtures of water and IPA.

ACKNOWLEDGEMENTS

This work was supported by 1) Korea Institute of Energy Technology Evaluation and Planning (KETEP) and the Ministry of Trade, Industry & Energy (MOTIE) of the Republic of Korea (No. 20194010201840), 2) Technology Innovation Program (20010846, Development of nano sized bio filter and module for virus removal) funded by the Ministry of Trade, Industry & Energy (MOTIE, Korea).

CONFLICTS OF INTEREST

There are no conflicts of interest to declare.

REFERENCES

1. P. Das, S. K. Ray, S. Kuila, H. Samanta and N. Singha, *Sep. Purif. Technol.*, **81**, 159 (2011).
2. F. Kursun, *J. Mol. Struct.*, **1201**, 127170 (2020).
3. S. Chaudhari, Y. Kwon, M. Moon, M. Shon, S. Nam and Y. Park, *J. Appl. Polym. Sci.*, **134**, 45572 (2017).
4. K. Sawamura, T. Furuhata, Y. Sekine, E. Kikuchi, B. Subramanian and M. Matsukata, *Appl. Mater. Interfaces*, **7**, 13728 (2015).
5. M. Dmitrenko, A. Penkova, A. Kuzminova, M. Morshed, M. Larionov, H. Alem, A. Zolotarev, S. Ermakov and D. Roizard, *Appl. Surf. Sci.*, **450**, 527 (2018).
6. B. Bolto, M. Hoang and Z. Xie, *Chem. Eng. Process. Process Intensif.*, **50**, 227 (2011).
7. P. D. Chapman, T. Oliveira, A. G. Livingston and K. Li, *J. Membr. Sci.*, **318**, 5 (2008).
8. J. G. Wiljmans and R. W. Baker, *J. Membr. Sci.*, **107**, 1 (1995).
9. Y. Ong, G. Shi, N. Le, Y. Tang, J. Zuo, S. Nunes and T. Chung,

Prog. Polym. Sci., **57**, 1 (2016).
10. E. Halakoo and X. Feng, *Chem. Eng. Sci.*, **216**, 115488 (2020).
11. G. Yang, Z. Xie, C. Doherty, M. Cran, D. Cran, D. Ng and S. Gray, *J. Membr. Sci.*, **603**, 118005 (2020).
12. H. Sun, D. Sun, X. Shi, B. Li, D. Yue, R. Xiao, P. Ren and J. Zhang, *Sep. Purif. Technol.*, **241**, 116739 (2020).
13. F. Kurşun and N. Işıklan, *J. Ind. Eng. Chem.*, **41**, 91 (2016).
14. C. Prasad, B. Yeriswamy, H. Sudhakar, P. Sudhakara, M. Subha and J. Song, *J. Appl. Polym. Sci.*, **125**, 3351 (2012).
15. N. Ghobadi, T. Mohammadi, N. Kasiri and M. Kazemimoghadam, *J. Appl. Polym. Sci.*, **134**, 44587 (2017).
16. N. D. Hilmioglu and S. Tulbentci, *Desalin. Water Treat.*, **48**, 191 (2012).
17. P. Das, S. K. Ray, S. B. Kuila, H. S. Samanta and N. R. Singha, *Sep. Purif. Technol.*, **81**, 159 (2011).
18. L. Ye, Q. Lin, Q. Zhang, A. Zhu and G. Zhou, *J. Appl. Polym. Sci.*, **105**, 3640 (2007).
19. M. Nemati, S. Hosseini and M. Shabanian, *J. Korean Chem. Eng.*, **34**, 1813 (2017).
20. S. Hosseini, H. Alibakhshi, E. Jashni, F. Parvizian, J. Shen, M. Taheri, M. Ebrahimi and N. Rafiei, *J. Hazard. Mater.*, **381**, 12884 (2020).
21. K. Kim, P. Ingole and H. Lee, *Int. J. Hydroen Energy*, **42**, 24205 (2017).
22. P. Ingole, M. Baig, W. Choi, X. An, W. Choi, J. Jeon and H. Lee, *Chem. Eng. Res. Des.*, **127**, 45 (2017).
23. O. Choi, P. Ingole and H. Lee, *Sep. Purif. Technol.*, **211**, 401 (2019).
24. V. Freger, E. Korin, J. Wisniak and E. Korngold, *J. Membr. Sci.*, **164**, 251 (2000).
25. Y. Zhai, B. Zhang, X. Fu and Z. Tong, *Sep. Purif. Technol.*, **234**, 116093 (2020).
26. Q. Zhao, Q. An, Y. Ji, J. Qian and C. Gao, *J. Membr. Sci.*, **379**, 19 (2011).
27. D. Achari, P. Rachipudi, S. Naik, R. Kruppannan and M. Karidura-ganavar, *J. Ind. Eng. Chem.*, **78**, 383 (2019).
28. G. Shi, J. Zuo, S. Tang, S. Wei and T. Chung, *Sep. Purif. Technol.*, **140**, 13 (2015).
29. S. Kononova, A. Volodko, V. Petrova, E. Kruchinina, Y. Baklagina, E. Chusovitin and Y. Skorik, *Carbohydr. Polym.*, **181**, 86 (2018).
30. C. Hu, B. Li, R. Guo, H. Wu and Z. Jiang, *Sep. Purif. Technol.*, **55**, 327 (2007).
31. S. William, J. Hummers and R. E. Offeman, *J. Am. Chem. Soc.*, **80**, 1339 (1958).
32. J. Wu, C. Ye, W. Zhang, N. Wang, K. Lee and Q. An, *J. Membr. Sci.*, **577**, 104 (2019).
33. S. Chaudhari, Y. Kwon, M. Shon, S. Nam and Y. Park, *J. Ind. Eng. Chem.*, **81**, 185 (2020).
34. K. Zhang, R. Hu, G. Fan and G. Li, *Sens. Actuators, B: Chem.*, **243**, 721 (2017).
35. M. Sumathra, K. Sadasivni, S. Kumar and M. Rajan, *ACS Omega*, **3**, 14620 (2018).
36. Y. Jiang, J. Gong, G. Zeng, X. Ou, Y. Chang and C. Deng, *Int. J. Biol. Macromol.*, **82**, 486 (2016).
37. T. Yan, H. Zhang, D. Huang, S. Feng, M. Fujita and X. Gao, *Nanomaterials*, **7**, 59 (2017).
38. R. Bryaskova, N. Georgieva, T. Andreeva and R. Tzoneva, *Surf. Coat. Technol.*, **235**, 186 (2013).
39. H. Pingan, J. Mengjun, Z. Yanyan and H. Ling, *RSC Adv.*, **7**, 2450 (2017).
40. A. Wach, M. Drozdek, B. Dudek, E. Szneler and P. Kustrowski, *Catal. Commun.*, **64**, 52 (2015).
41. P. Zuo, H. Feng, Z. Xu, L. Zhang, Y. Zhang, W. Xia and W. Zhang, *Chem. Cent. J.*, **7**, 39 (2013).
42. Z. Xing, Z. Ju, Y. Zhao, J. Zhu, Y. Zhu, Y. Qiang and Y. Qian, *Nat. Sci. Rep.*, **6**, 26146 (2016).
43. Z. Liu, Z. Zhao, Y. Wang, S. Dou, D. Yan, D. Liu, Z. Xia and S. Wang, *Adv. Mater.*, **29**, 1606207 (2017).
44. M. Schnucklake, L. Eifert, J. Schneider, R. Zeis and C. Roth, *Beilstein J. Nanotechnol.*, **10**, 1131 (2019).
45. P. Shao and R. Huang, *J. Membr. Sci.*, **287**, 162 (2007).
46. B. Tieke, F. Ackern, L. Krasemann and A. Toutianoush, *Euro. Phys. J. E*, **5**, 29 (2001).
47. K. Cao, Z. Jiang, J. Zhao, C. Zhao, C. Gao, F. Pan, B. Wang, X. Cao and J. Yang, *J. Membr. Sci.*, **469**, 272 (2014).
48. Y. Wang, S. Goh, T. Chung and P. Na, *J. Membr. Sci.*, **326**, 222 (2009).
49. K. Kim, P. Ingole, J. Kim and H. Kim, *Chem. Eng. J.*, **233**, 242 (2013).
50. P. Ingole and N. Ingole, *Korean J. Chem. Eng.*, **31**, 2109 (2014).
51. B. Liang, W. Zhan, G. Qi, S. Lin, Q. Nan, Y. Liu, B. Cao and K. Pan, *J. Mater. Chem., A*, **3**, 5140 (2015).
52. Y. Han, K. Wang, J. Lai and Y. Liu, *J. Membr. Sci.*, **463**, 17 (2014).
53. S. Mosleh, T. Khosravi, O. Bakhtiari and T. Mohammadi, *Chem. Eng. Res. Des.*, **90**, 433 (2012).